



In situ construction of a novel Bi/CdS nanocomposite with enhanced visible light photocatalytic performance

Bo Wang, Wenhui Feng, Lulu Zhang, Yan Zhang, Xueyan Huang, Zhibin Fang, Ping Liu *

Research Institute of Photocatalysis, State Key Laboratory of Photocatalysis on Energy and Environment, Fuzhou University, Fuzhou 350002, PR China

ARTICLE INFO

Article history:

Received 27 November 2016

Received in revised form 9 January 2017

Accepted 18 January 2017

Available online 18 January 2017

Keywords:

Bi/CdS nanocomposite

Semimetal

Degradation

Visible light photocatalysis

Charge transfer

ABSTRACT

A novel Bi/CdS nanocomposite is obtained via an in-situ chemical reduction method under mild conditions. The incorporation of Bi nanostructure can significantly enhance the photocatalytic performance for methyl orange (MO) and salicylic acid (SA) degradation compared with pristine CdS under visible light irradiation. The dramatically improved photoactivity can be attributed to the enhanced light absorption and optimized charge separation. In addition, the photocatalysis mechanism upon Bi/CdS for MO degradation is also investigated. This study is hoped to provide a new inspiration for the construction of high-efficiency semimetal/semiconductor photocatalysts, especially for non-noble metal/M_xS_y nanocomposites.

© 2017 Elsevier B.V. All rights reserved.

1. Introduction

Semiconductor photocatalysis technology has been evolving as a promising and environmentally friendly technology for selectively organic synthesis [1,2], water splitting [3–5], and environmental purification [6–8] by utilizing light energy. Although more and more photocatalysts have been developed during the past decades, low quantum efficiency is still a bottleneck for photocatalysis technology [9–11]. As we known, photocatalytic efficiency is influenced by many factors. The spectral response range and the charge carriers separation efficiency are identified as two of the most key among various factors. Therefore, it is of great significance to develop highly efficient visible-light-driven photocatalysts with superior charge separation efficiency.

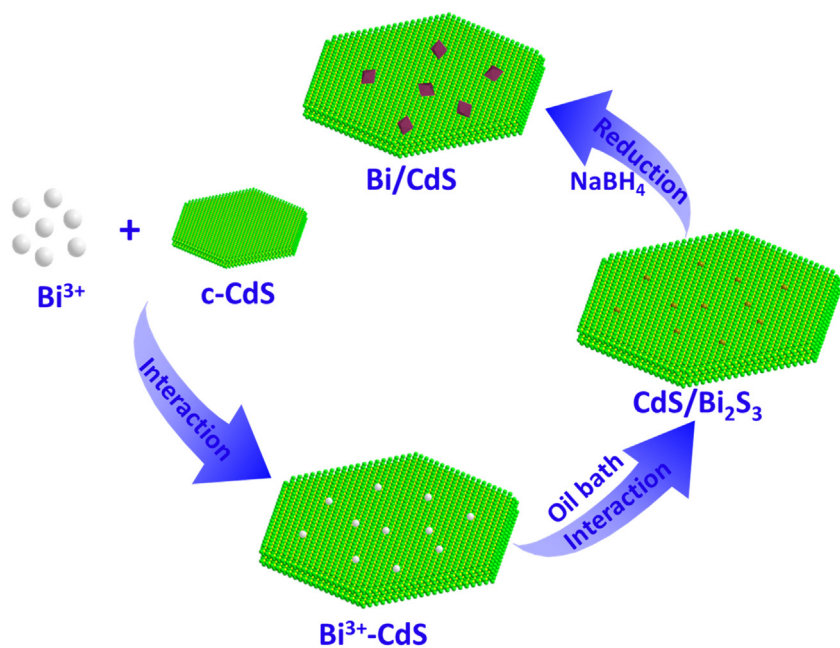
Hitherto, various types of visible-light driven photocatalysts such as metal oxides (Cu₂O, Fe₂O₃ and WO₃) [12–14], metal sulfides (Cu₂S, CdS and In₂S₃) [15–18], Bi-based materials (Bi₂WO₆, BiOBr and BiOI) [19–21], and g-C₃N₄-based materials [22] have been developed in order to efficiently utilize the visible light in the solar spectrum. Specifically, CdS, as one of the most attractive narrow-band semiconductor photocatalyst, has been widely studied in photocatalytic applications because of its unique optical and electrical properties [23–26]. Regrettably, the extremely fast recombination rate of photo-induced carriers and photocorro-

sion of CdS photocatalyst are still the mainly barriers which hinder its wider application [27,28]. Thus, the promotion for the separation of the electron–hole pair is crucially important to enhance the photocatalytic performance of CdS-based photocatalysts.

Up to now, for the sake of promoting separation of the photo-generated electron–hole pair in CdS-based photocatalysts, a great deal of effort has been made by scientists, including noble metal modification, graphene modification, transition-metal sulfides modification [29–32], etc. Among them, noble metal nanoparticles (such as Pt [33], Au [34], Ag [35], Pd [36], etc.) modification has been widely used to improve the photocatalytic performance of semiconductor. Generally, a Schottky barrier can be built on the interface between metal and semiconductor photocatalyst, which would effectively promote the charge carriers separation, resulting the dramatically improved photocatalytic performance for the metal/semiconductor composite [33,34]. However, the high cost and scarcity of these noble metals may limit their practical application. Therefore, semimetal bismuth (Bi) has attracted a great deal of attention due to its unique advantages of low cost, easy availability, and superior transport properties recently. Besides, Bi nanoparticles exhibit plasmonic properties as noble metal nanoparticles [35]. As a promising substitute for noble metals, Bi nanostructure in above-mentioned systems can act as an excellent electron trap to facilitate the electron–hole separation in the photocatalytic process. For instance, we reported that a Bi/BiOCl nanocomposite exhibited a significantly improved photocatalytic performance [36]. Successively, such a phenomenon has also been observed in Bi/Bi₂O₃ [37], Bi/(BiO)₂CO₃, Bi/Bi₂MoO₆ [38], and Bi/C₃N₄ [39] photocatalyst sys-

* Corresponding author.

E-mail address: liuping@fzu.edu.cn (P. Liu).



Scheme 1. Schematic synthesis process of the Bi/CdS nanocomposites.

tems. However, the reported photocatalytic system integrating Bi with non-Bi-based semiconductor is scarce. It is probably due to the lack of an effective synthesis method for constructing the intimate interface between Bi and non-Bi-based semiconductor. Moreover, the inherent Bi element in Bi-based semiconductor may lead to a disturbance for exact understanding of the role of Bi nanoparticles as cocatalyst. Thus, developing a way to fabricate Bi/CdS with intimate interface would be a key step. Theoretically, once a Schottky barrier is built in the interface between Bi and CdS, semimetal Bi would accelerate the charge carriers separation of CdS. Therefore, Bi/CdS will be expected to be an excellent photocatalyst.

Herein, we have developed an in-situ chemical reduction method to assemble Bi on the CdS surface at low temperature based on an ion-exchange process. The novel Bi/CdS nanocomposites exhibit significantly enhanced photocatalytic capability and high stability for methyl orange (MO) and salicylic acid (SA) degradation under visible light irradiation. This work may provide a new inspiration for the construction of Bi/CdS with tight contact and advance the development of other non-noble metal/M_xS_y semiconductor nanocomposites. Further, this work would demonstrate the role of Bi in Bi/semiconductor system.

2. Experimental

2.1. Materials

Bismuth nitrate pentahydrate (Bi(NO₃)₃·5H₂O), ethylene glycol (EG), sodium borohydride (NaBH₄), ethanol (C₂H₆O) and methyl orange (MO) were purchased from Sinopharm Chemical Reagent Co., Ltd. (Shanghai, China). Additionally, cadmium sulfide (CdS) was purchased from Aladdin. All of the chemicals were analytical grade and used without any purification. Deionized (DI) water was used throughout this study.

2.2. Synthesis of Bi/CdS

The Bi/CdS was synthesized via an in situ chemical reduction reaction, as shown in **Scheme 1**. In a typical process, 1 g commercial CdS powders (c-CS) were dispersed to 50 mL ethylene glycol solution (50%, v/v) containing a certain amount of Bi(NO₃)₃·5H₂O.

After stirring for 15 min, the mixture was maintained at 80 °C for 1 h with magnetic stirring. And the products were washed with ethanol and deionized water for several times and dried at 60 °C for 4 h. The resulting powders were slowly added to 50 mL 1 M NaBH₄ solution under stirring. After stirring for 4 h at room temperature, the solid products were filtered and washed with deionized water for several times, and then dried at 60 °C for 12 h to obtain the final Bi/CdS products. The theoretical mass ratios of Bi to CdS were 10, 20, 30, and 50%, and the corresponding Bi/CdS photocatalysts were defined as B-CS-10, B-CS-20, B-CS-30, and B-CS-50, respectively.

2.3. Characterization

The crystal structure and purity of the products in this work were characterized by X-ray diffraction (XRD) patterns, which were obtained on a Bruker D8 Advance X-ray diffractometer with Cu K α radiation carried out at 40 mA and 40 kV in the 2 θ range of 10–80°. The morphology and microstructure of the as-prepared samples were analyzed by field-emission scanning electron microscope (FESEM, FEI Nova NanoSEM-230) and transmission electron microscope (TEM, Tecnai G2F20 S-TWIN, FEI Company). The accelerating voltage was 200 kV. X-ray photoelectron spectroscopy (XPS, Thermo ESCALAB 250XI) was utilized to study the chemical composition and the valence state of samples. The optical properties of the obtained products were investigated via UV-vis diffuse reflectance spectroscopy recorded by using a UV-vis-NIR spectrophotometer (Varian Cary-500). In which BaSO₄ acted as the reflectance standard. Photoluminescence spectra were also obtained using a Horiba Jobin-Yvon Fluorolog-3 spectrofluorometer with a 312 nm excitation wavelength. A ZENNIMUM electrochemical workstation (Zahner, Germany) was used for measurements of the electrochemical impedance spectroscopy (EIS).

2.4. Photocatalytic activity measurements

The photocatalytic activity of the synthesized Bi/CdS samples was evaluated by the photodegradation of methyl orange (MO, 10 mg/L) or salicylic acid (SA, 20 mg/L) under visible light irradiation. In a typical measurement, 0.08 g of photocatalyst was added to 80 mL of simulating pollutant solution in a 100 mL Pyrex glass

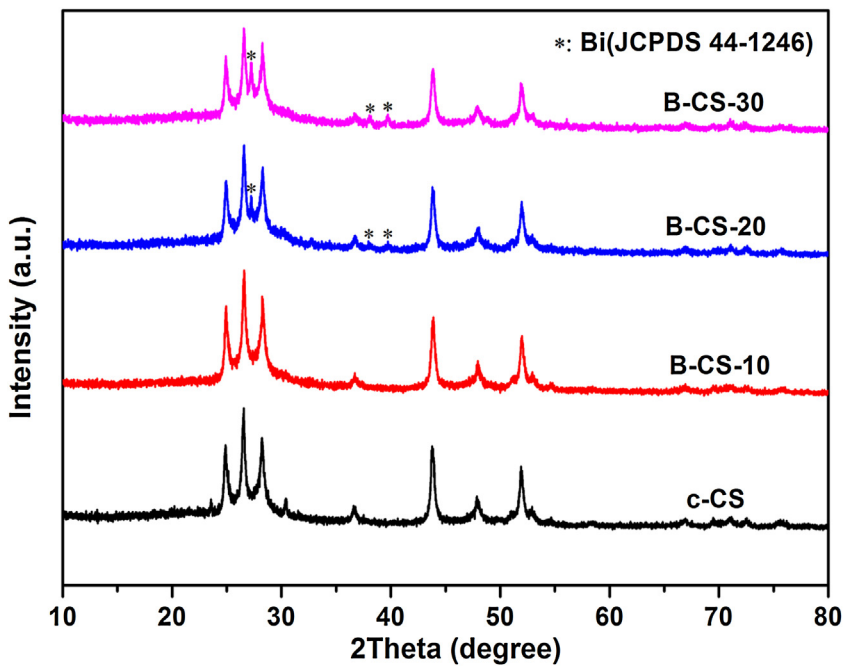


Fig. 1. XRD patterns of pure CdS and the as-prepared Bi/CdS nanocomposites.

vessel with a plane side. The 300W xenon lamp (PLS-SXE300, Beijing Perfect-Light Co. Ltd.) with a UV-cutoff filter (420 nm) was employed as the light source. The light intensity has been measured and shown in Fig. S1. To establish an adsorption-desorption equilibrium, the suspensions would be magnetically stirred in the dark for 60 min before illumination. At certain irradiation time intervals, 3 mL of the mixed solution was sampled and centrifuged, then analyzed using a Varian Cary-50 UV-vis spectrometer.

3. Results and discussion

3.1. Phase structure and morphology

The XRD patterns of commercial CdS and the as-prepared Bi/CdS samples are shown in Fig. 1. The main diffraction peaks of the samples indicate that CdS is crystallized in hexagonal wurtzite structure (JCPDS no. 77-2306, $a=4.136\text{ \AA}$ and $c=6.713\text{ \AA}$) [40], and Bi deposition process does not make any change to the crystal structure of CdS. With the increase of Bi content, the diffraction peaks of the rhombohedral phase Bi (JCPDS no. 44-1246) are more clearly shown at 27.2° , 37.9° and 39.6° in the XRD pattern of B-CS-30, indicating that Bi metal is successfully introduced into the composites [36]. Besides, no other impurities peaks are detected, which demonstrated that Bi/CdS samples are achieved.

The morphologies of the CdS and Bi/CdS samples were investigated by SEM images. As shown in Fig. 2a and b, both CdS and Bi/CdS are irregular aggregates, which is consisted of a great quantity of nanoparticles with sizes of 10–100 nm. It indicates that the introduction of Bi does not change obviously the morphology or particle size of CdS. Moreover, the EDX mapping of the B-CS-30 sample is displayed in Fig. S2, the result further demonstrates that the S, Cd, Bi, and O elements coexist in B-CS-30 and the Bi nanoparticles are well distributed in the composite.

TEM and HRTEM were carried out to further characterize the as-prepared Bi/CdS composite. It can be seen in Fig. 2c, Bi nanoparticles with size of about 20 nm have been successfully deposited on the surface of CdS nanoparticles. Three kinds of lattice fringes with interplanar spacings of about 0.335, 0.357, and 0.325 nm, corresponding to the (100), (002) lattice plane of CdS, and the (012)

lattice plane of metallic Bi respectively, are observed in HRTEM images (Fig. 2d). Combined with the XRD patterns, these results could confirm that metallic Bi nanoparticles are indeed deposited on the surface of CdS via the in situ chemical reduction of Bi^{3+} ions by NaBH_4 solution.

3.2. Chemical composition

The XPS spectra were used to investigate the surface chemical composition of the Bi/CdS samples and pure CdS. The survey scan XPS spectra in Fig. 3a shows that the B-CS-30 sample contains Bi, S, O, and Cd elements, while the pristine CdS does not contain Bi. The C 1s peak in the spectrum of both CdS and B-CS-30 can be attributed to adventitious carbon. The S 2s peaks for both CdS and B-CS-30 samples located at 225.8 eV (Fig. 3b), those are attributed to the Cd-S bonds in both CdS and B-CS-30 [41]. Fig. 3c exhibits the high-resolution Cd 3d XPS spectra of both CdS and B-CS-30. For the bare CdS sample, two strong peaks at the binding energies of 412.1 and 405.3 eV are ascribed to $\text{Cd 3d}_{3/2}$ and $\text{Cd 3d}_{5/2}$ respectively, which suggests that Cd^{2+} in CdS is not reduced during chemical reduction process [42]. Notably, after Bi loading, an obvious shift for about 0.21 eV toward the higher binding energies can be observed in Cd 3d peaks of the B-CS-30 sample as compared to those of original CdS sample. This shift indicates the existence of a strong interfacial interaction between Bi and CdS [43]. The Bi 4f XPS spectra of the B-CS-30 display visible differences before and after etching (Fig. 3d). The peaks at the binding energies of 162.1 and 156.7 eV can be assigned to the Bi–Bi bonds of the metallic Bi, while other two peaks located at 164.1 and 158.8 eV would be attributed to the Bi^{3+} in bismuth oxides [44]. Significantly enhanced Bi–Bi peaks can be observed after surface etching, indicating the formation of a thin bismuth oxide layer on the surface of the metallic Bi. The oxide layer can inhibit the further oxidation of the Bi metal. The Bi–O bonds can still be observed at the sublayer, which means that a new bismuth oxide layer would be formed due to the exposure after etching for the metallic Bi. Two peaks around 530.8 and 529.6 eV (Fig. 3e) are assigned to the adsorbed oxygen species on the surface and the Bi–O bond in bismuth oxides, respectively [45]. Moreover, the intensity of O 1s XPS peaks is distinctly reduced after surface etching with

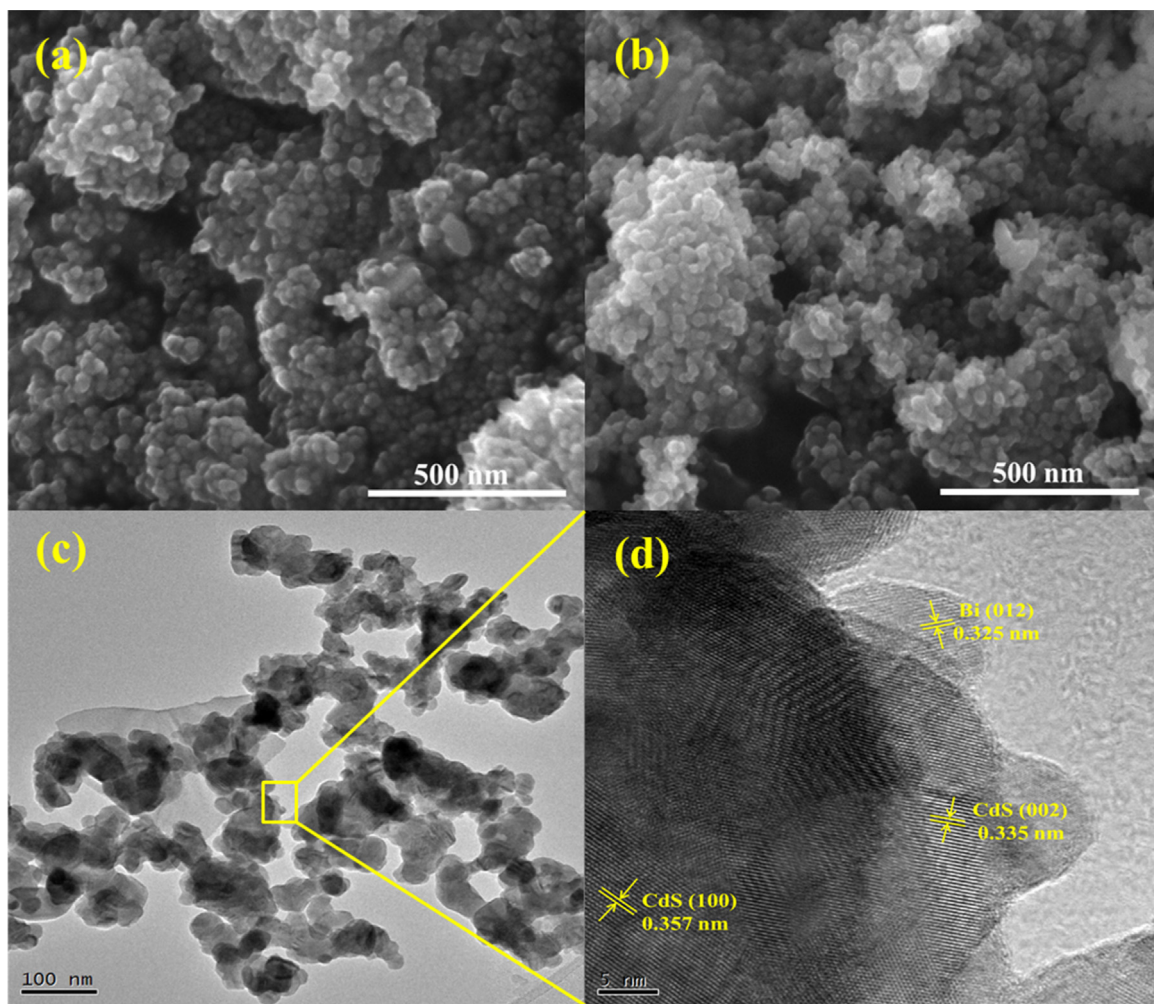


Fig. 2. Typical SEM images of (a) pure CdS and (b) B-CS-30 nanocomposite; (c) TEM and (d) HRTEM images of B-CS-30 sample.

a depth of 4 nm, suggesting that the oxide layer is only formed on the surface. These results of XPS data analysis indicate that CdS and Bi metal coexisted in the Bi/CdS hybrid materials, also reveals the existence of a strong interfacial interaction between the metallic Bi and CdS.

3.3. Photocatalytic activity and stability

The above results show that we effectively construct Bi/CdS materials with close contact interface. In order to verify our hypothesis, the photocatalytic capability of the Bi/CdS nanocomposites has been evaluated by the degradation of MO or SA at room temperature. As shown in Fig. 4a, only 28.5% MO can be degraded by pure CdS powders after 50 min irradiation. The photocatalytic activity of CdS is greatly enhanced by the introduction of a certain amount of Bi nanoparticles on the surface of CdS. It is clear to see that the B-CS-30 sample exhibits the highest photocatalytic activity with the MO degradation ratio of 93.7% after 50 min irradiation. Notably, the MO degradation ratio decreased sharply when the Bi loading further increases to 50%, which may be attributed to the shielding effect of Bi particles, but it is still more efficient than that of bare CdS powders. This similar phenomenon has been widely found in previous works [36,39,46]. Besides, for comparison, blank experiment was executed without any photocatalyst at the same conditions. As a result, no obvious decoloration for MO solution is observed after illumination for 50 min. To further understand the photocatalytic efficiency of the samples, the photocatalytic degra-

dation kinetics of MO under visible light irradiation is investigated. As can be seen in Fig. 4b, the process is fitted to pseudo-first-order kinetics based on the equation of $\ln(C/C_0) = kt$ [47], the apparent rate constants k have been calculated and shown in Table S1 and inset in a histogram graph form in Fig. 4b. The B-CS-30 material has the maximum apparent rate constant of 0.0625 min^{-1} , which is 9.33 times higher than that of pure CdS. To test the stability of the Bi/CdS composites, the B-CS-30 sample was collected after each MO photodegradation reaction for the subsequent recycling experiment under visible light irradiation. It can be found in Fig. 5, no apparent decrease of the photocatalytic efficiency is observed after four consecutive cycles, which indicates the Bi/CdS hybrid materials have high stability and reusability during the photocatalysis reaction.

Moreover, in order to further eliminate the influence of dye sensitization effect in photocatalytic process, we also used the degradation of colorless SA under visible light irradiation. The result has been shown in Fig. 4c. It is clear that the Bi/CdS nanocomposites exhibit much enhanced photocatalytic performance than that of pure CdS. The corresponding photocatalytic degradation kinetics have been investigated and shown in Fig. 4d, meanwhile, the apparent rate constants k are also calculated and displayed in inset. The apparent rate constant of B-CS-30 is 1.69 times higher than that of pure CdS. The findings confirm that the dye-sensitization effect is not the main factor for the B-CS-30 samples because the colorless SA cannot absorb the visible light.

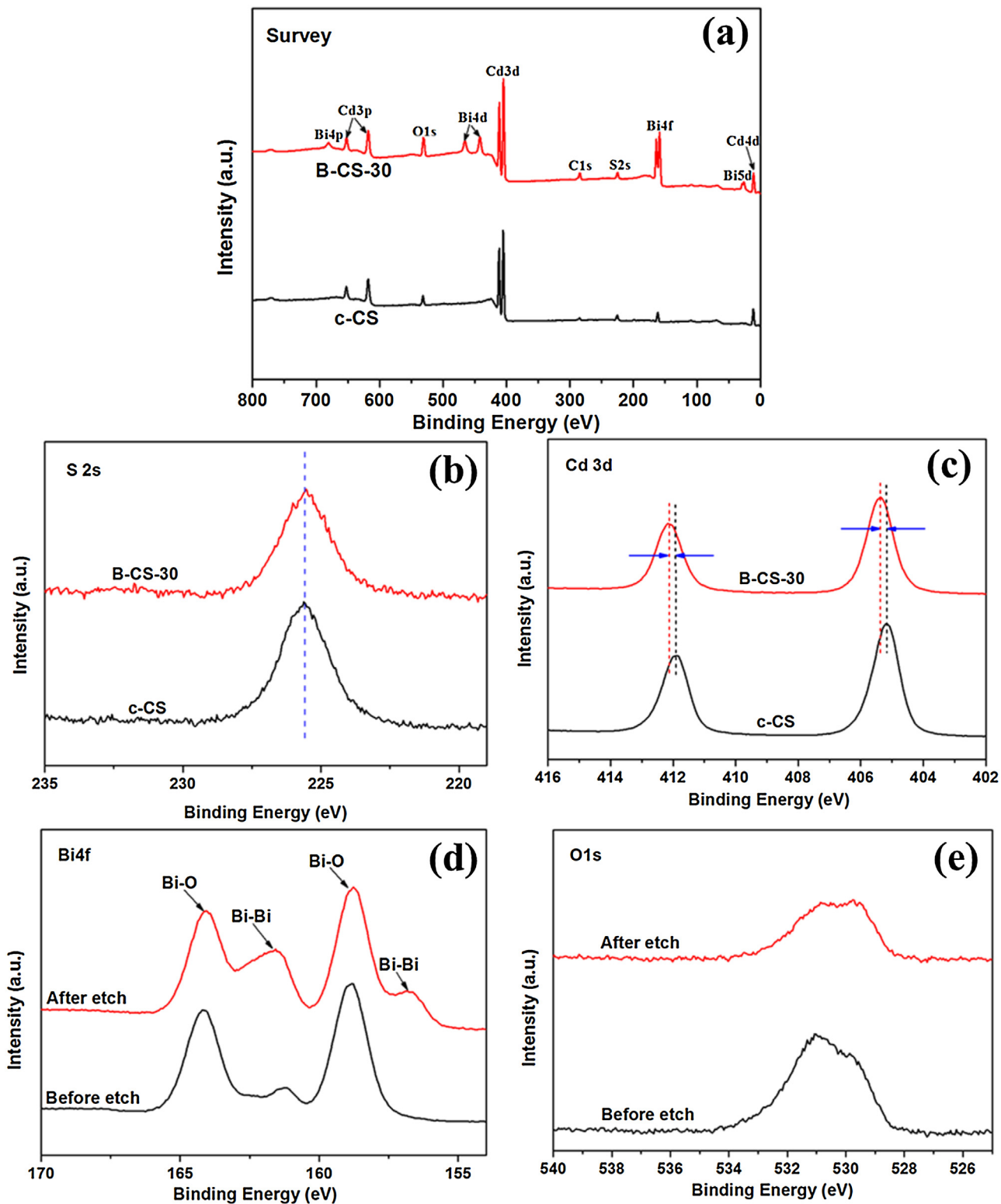


Fig. 3. XPS spectra of pure CdS and the B-CS-30 sample: (a) Survey of the sample, (b) S 2s, (c) Cd 3d, and the XPS spectra of the B-CS-30 material: (d) Bi 4f, (e) O 1s before and after etching.

3.4. Optical properties and charge separation

In order to understand the reasons for the enhanced photo-catalytic capability of the Bi/CdS nanocomposites under visible light irradiation, the light properties of both pure CdS and the as-prepared Bi/CdS samples have been investigated via DRS. The

corresponding UV-vis diffuse reflectance spectra are displayed in Fig. 6, pristine CdS sample can only absorb visible light below 530 nm. This absorption can be assigned to the charge transfer in the band gap of CdS. Obviously, a significantly enhanced light absorption with the wavelength range of 530–800 nm can be observed after the introduction of Bi nanoparticles. The light

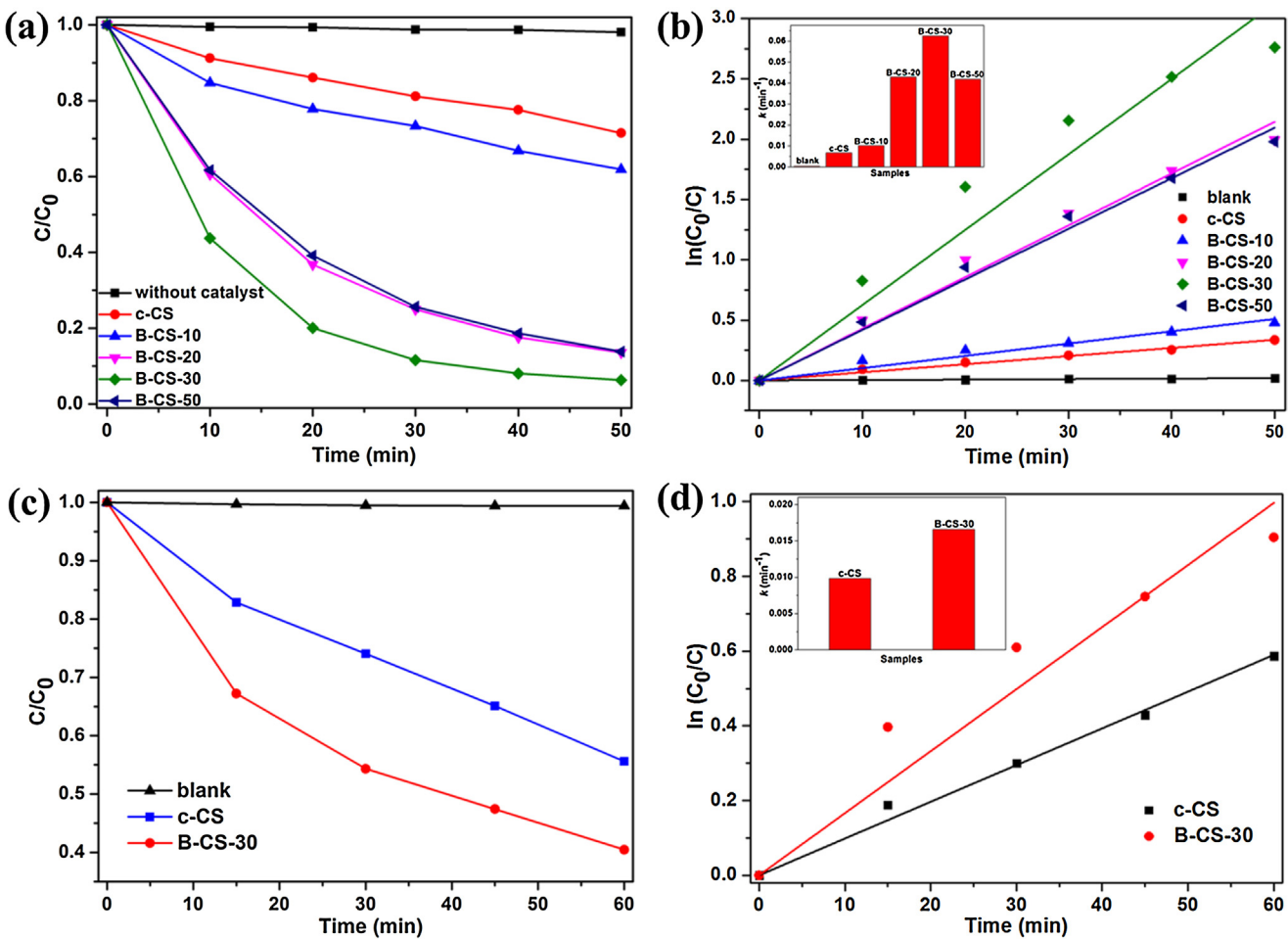


Fig. 4. (a) Concentration changes of MO in pristine CdS and Bi/CdS nanocomposites suspensions under visible light irradiation ($\lambda > 420$ nm); (b) Kinetic linear simulation curves for the degradation of MO under visible light irradiation. Insert: the corresponding degradation rate constant k of samples; (c) Photodegradation of SA in the presence of pristine CdS and B-CS-30 nanocomposites under visible light irradiation ($\lambda > 420$ nm); (d) Kinetic linear simulation curves for the degradation of SA under visible light irradiation. Insert: the corresponding degradation rate constant k of samples.

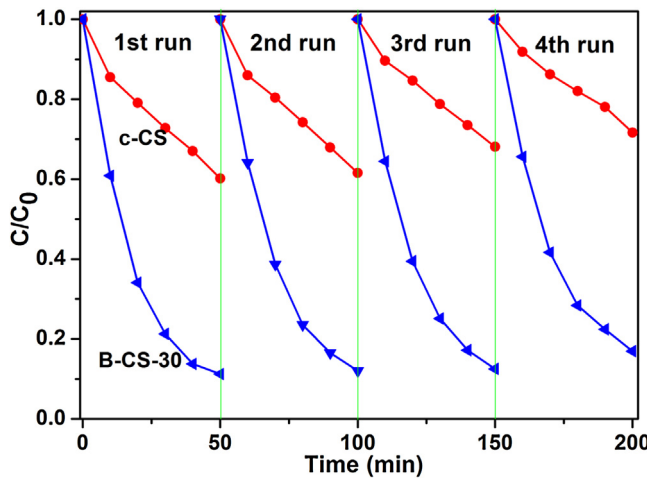


Fig. 5. Cycling runs for the photocatalytic degradation of MO in B-CS-30 nanocomposite suspensions under visible light irradiation.

absorption intensity of the Bi/CdS nanocomposites can be adjusted by changing the amount of Bi. Such absorption was accordance with the color transition of the samples from light yellow to dark green (Fig. S3). The results imply that the introduction of Bi nanoparticles into the CdS can remarkably improve the visible-light absorption

of the Bi/CdS nanocomposites, which may result in the enhanced photocatalytic activity of the samples [48]. The enhanced light absorption could be ascribed to metallic Bi with a black color. Besides, the SPR absorptions of Bi nanoparticles (10–70 nm in size) centered at around 500 nm has been discovered because of the SPR and light scattering [49]. Although the SPR absorptions of metallic Bi are not observed in our work due to the disturbance of the absorption edge, the enhanced visible light absorption may be associated with the SPR property of metal Bi to some extent.

To investigate the separation efficiency of the charge carriers in photocatalysts, the photoluminescence (PL) spectra of both B-CS-30 samples and pristine CdS has been measured and shown in Fig. 7a [36,50]. The pristine CdS displays a strong emission peak excited at 312 nm, while the B-CS-30 samples exhibit a sharply weakened PL intensity, demonstrating that the recombination of charge carriers is markedly inhibited after the introduction of Bi. The metallic Bi with high electron conductivity can serve as an electron trap via the Schottky barrier formed at the interface of the metal-semiconductor hybrid materials, which should be responsible for this result [51,52]. As a consequence, the electrons transfer from the conduction band (CB) of CdS to the Bi metal, which improves the separation and lifetime of photoinduced electron–hole pairs [36,53], and thus promotes the photoactivity of the Bi/CdS nanocomposites.

In addition, in order to further investigate the interfacial charge transfer properties, electrochemical impedance spectroscopy (EIS)

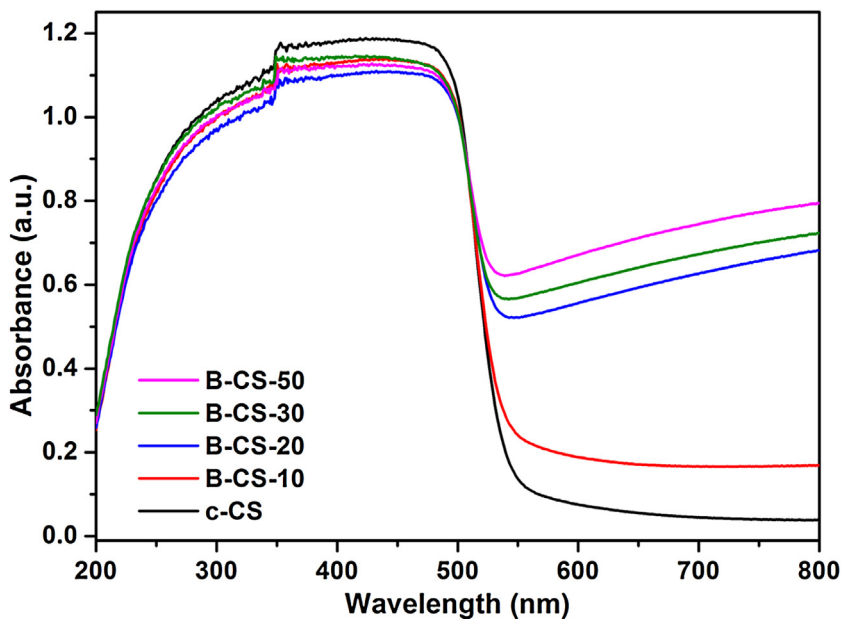


Fig. 6. UV-vis DRS patterns of pure CdS and the as-prepared Bi/CdS materials.

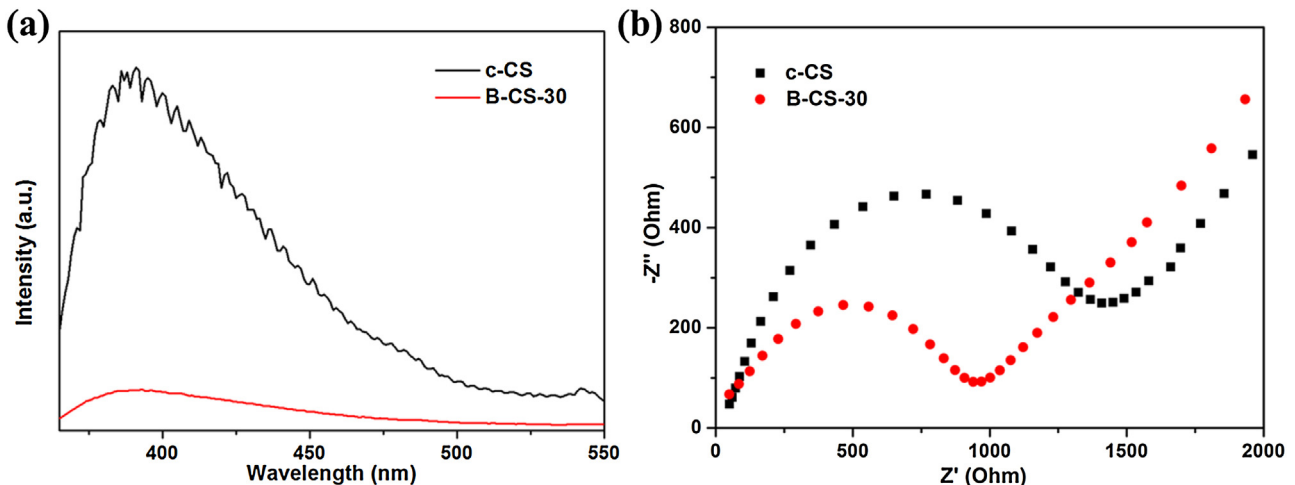


Fig. 7. (a) PL spectra and (b) Electrochemical impedance spectroscopy of bare CdS and the as-prepared B-CS-30 samples.

of both bare CdS and B-CS-30 samples is carried out and shown in Fig. 7b. In general, a small radius of the semicircle in the Nyquist plot means a low resistance [54,55]. It is found that the B-CS-30 nanocomposite has a smaller radius of the semicircle arc in the Nyquist plot than that of pristine CdS, which signifies that Bi as a typical semimetal can facilitate the interfacial charge transfer and lead to an effective separation of photoinduced electrons and holes [36]. These results are in accordance with the PL data analysis above, which confirm that the introduction of Bi metal can improve photocatalytic efficiency effectively.

3.5. Photocatalytic mechanism

The kind and amount of reactive species mainly dominate the degradation rate of organic pollutants. A series of active species trapping experiments were carried out to reveal the role of the primary active radical species on the photocatalysis reaction over Bi/CdS nanocomposites (Fig. 8). When ammonium oxalate (AO) as a holes (h^+) scavenger is added into the photodegradation system [56], the removal rate of MO over B-CS-30 is dramatically

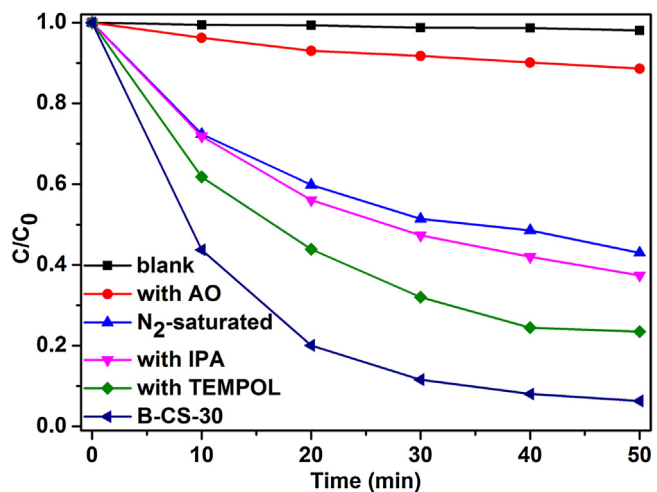


Fig. 8. Photocatalytic degradation of MO by the B-CS-30 nanocomposite in the presence of different scavengers.

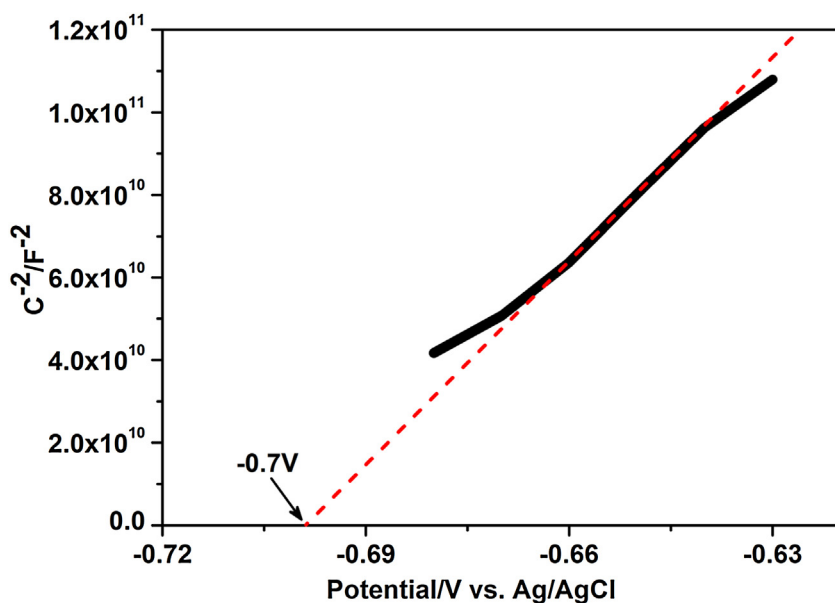


Fig. 9. Mott-Schottky plot for CdS in 0.2 M Na_2SO_4 aqueous solution ($\text{pH} = 6.8$).

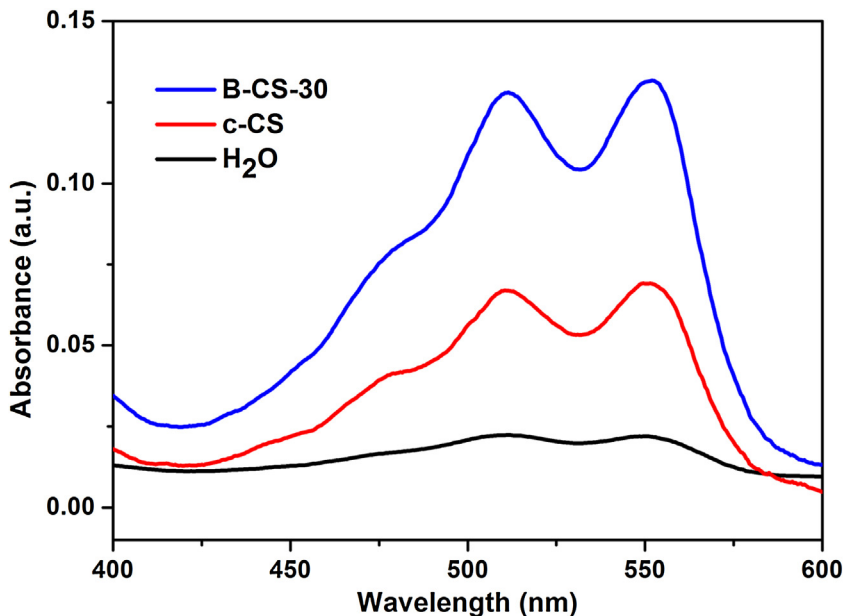
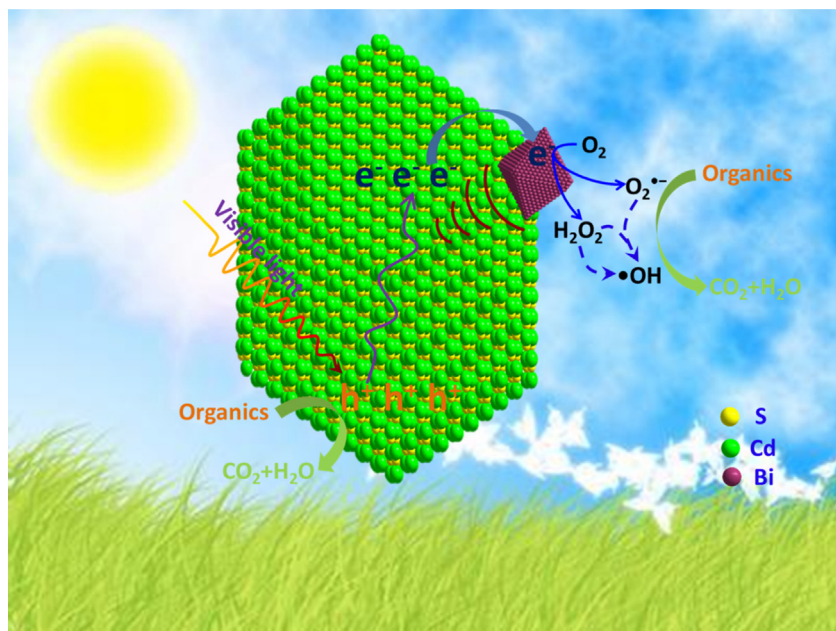


Fig. 10. Absorption spectra of the DPD/POD reagent in different samples aqueous dispersions after 30 min of visible light irradiation.

decreased, which suggests the significance of photogenerated holes in the photocatalytic degradation process. After isopropyl alcohol (IPA) as a hydroxyl radicals ($\cdot\text{OH}$) scavenger is added into the solution [57], the degradation rate of MO is also greatly reduced, but the inhibition extent is less than the case when the AO is added. It is meant that the photogenerated holes play a more important role than hydroxyl radicals toward the decomposition of MO over Bi/CdS materials. The addition of TEMPOL or N_2 resulted in partial inhibition of the MO photodegradation [58], which further indicates that superoxide radical ($\text{O}_2^{\bullet-}$) or oxygen molecule also play a certain role in this system.

Moreover, to further understand the intrinsic mechanism, it is absolutely vital to locate the valence band (VB) and conduction band (CB) potentials of the Bi/CdS samples. The conduction band of B-CS-30 nanocomposite is measured by the Mott-Schottky plot and shown in Fig. 9. The result indicates that the flatband potential

of the B-CS-30 hybrid material is about -0.7 eV vs. Ag/AgCl, that is -0.5 eV vs. standard hydrogen electrode (SHE) [59], which is consistent with previously reported results [60,61]. Based on the DRS analysis in Fig. 6, the absorption edge of the samples is about 520 nm, revealing that the band gap energy (E_g) of bare CdS is about 2.4 eV. Thus, the valence band (VB) potential can be determined to be about 1.9 eV by using the equation $E_{\text{CB}} = E_{\text{VB}} - E_g$. This result is consistent with the XPS valence-band spectra of B-CS-30 material (Fig. S4). The VB potential (1.9 eV) is more negative compared with the redox potential for $\cdot\text{OH}/\text{OH}^-$ (+1.99 eV) [62], thus OH^- cannot be oxidized to $\cdot\text{OH}$ by the photogenerated holes of B-CS-30 hybrid material. Meanwhile, the O_2 can be reduced to yield $\text{O}_2^{\bullet-}$ or H_2O_2 due to the redox potential for $\text{O}_2/\text{O}_2^{\bullet-}$ (-0.33 eV) [62] or $\text{O}_2/\text{H}_2\text{O}_2$ ($+0.695$ eV) [63] is more positive than the CB potential (-0.5 eV) of CdS. In order to further uncover the role of oxygen on the photocatalytic process over B-CS-30, H_2O_2 is detected by



Scheme 2. Schematic illustration of the proposed mechanism for the degradation of MO over the Bi/CdS photocatalysts under visible light irradiation.

a common DPD-POD method [64]. The consequence is shown in Fig. 10, no obvious characteristic absorption peak assigned to H_2O_2 is observed for water in 30 min visible-light irradiation, while two absorption peaks at about 510 and 551 nm can be detected in bare CdS or the B-CS-30 aqueous dispersion under the same condition. It is clear that the amount of H_2O_2 generated in the B-CS-30 is larger than that in pristine CdS, which should be responsible for the enhanced photocatalytic activity.

The photocatalytic mechanism for the degradation of MO by the B-CS-30 composite could be illustrated in Scheme 2 based on the above experimental results and analysis. The SPR effect of Bi metal may induce a built-in electric field, which will accelerate the photoexcited electrons and holes separation, and thus improve photocatalytic activity [49,65,66]. The electrons are excited from the VB to the CB of CdS under visible light irradiation, leaving the holes on the VB. Then the photogenerated electrons tend to transfer to Bi metal due to their matched energy band and close interfacial contact. The adsorbed oxygen molecule can trap these electrons and be reduced to $\text{O}_2^{\bullet-}$ or H_2O_2 via a single-electron or two-electron path, and then the $\bullet\text{OH}$ can be formed by the reaction between $\text{O}_2^{\bullet-}$ or electrons and H_2O_2 [67]. The $\bullet\text{OH}$ with high reaction ability is considered a vital species in the photodegradation mechanism of MO. Meanwhile, although the high active photogenerated h^+ of the B-CS-30 cannot oxidize H_2O to generate $\bullet\text{OH}$ on account of the h^+ potential is negative than the redox potential for $\bullet\text{OH}/\text{OH}^-$, it can also directly oxidize the MO to H_2O and CO_2 . As a consequence, the above reactive species can effectively decompose the adsorbed MO molecule. In other words, the B-CS-30 composite displays a superior photocatalytic performance under visible light irradiation.

4. Conclusions

In summary, the Bi/CdS nanocomposites with excellent photocatalytic performance have been synthesized via an in-situ chemical reduction reaction based on a simply ion-exchange process. The metallic Bi particles are distributed evenly on the surface of CdS. The introduction of semimetal Bi significantly promotes the photocatalytic capacity of CdS for the degradation of MO and SA. The B-CS-30 exhibits the optimal photocatalytic activity and high

stability. The vital role of Bi for the enhanced photocatalytic performance can be ascribed to the enhanced light absorption and the superior charge separation efficiency. In addition, the photocatalysis mechanism is proposed based on active species trapping experiments, Mott–Schottky plot, and XPS valence spectra analysis. It is expected that this work could provide a new inspiration for the development of Bi/CdS and other non-noble metal/ M_xS_y semiconductor nanocomposites.

Acknowledgements

This work is supported by the National Natural Science Foundation of China (21473031, 21273035, 21673041 and 21173046), the National Basic Research Program of China (973 Program: 2013CB632405), the National Key Technologies R & D Program of China (2014BAC13B03) and the Science & Technology Plan Project of Fujian Province (2014Y2003).

Appendix A. Supplementary data

Supplementary data associated with this article can be found, in the online version, at <http://dx.doi.org/10.1016/j.apcatb.2017.01.047>.

References

- [1] K. Iwashina, A. Iwase, Y.H. Ng, R. Amal, A. Kudo, *J. Am. Chem. Soc.* 137 (2015) 604–607.
- [2] D.R. Gamelin, *Nat. Chem.* 4 (2012) 965–967.
- [3] C. Pan, D. Li, X. Ma, Y. Chen, Y. Zhu, *Catal. Sci. Technol.* 1 (2011) 1399–1405.
- [4] D. Ravelli, D. Dondi, M. Fagnoni, A. Albini, *Chem. Soc. Rev.* 38 (2009) 1999–2011.
- [5] M.G. Kibria, F.A. Chowdhury, S. Zhao, B. AlOtaibi, M.L. Trudeau, H. Guo, Z. Mi, *Nat. Commun.* 6 (2015) 6797.
- [6] H. Lee, W. Choi, *Environ. Sci. Technol.* 36 (2002) 3872–3878.
- [7] C. Chen, W. Ma, J. Zhao, *Chem. Soc. Rev.* 39 (2010) 4206–4219.
- [8] J. Schneider, M. Matsuoka, M. Takeuchi, J. Zhang, Y. Horiuchi, M. Anpo, D.W. Bahneemann, *Chem. Rev.* 114 (2014) 9919–9986.
- [9] I. Tsuji, H. Kato, A. Kudo, *Angew. Chem.* 44 (2005) 3565–3568.
- [10] H.B. Gray, *Nat. Chem.* 1 (2009) 7.
- [11] J. Ran, J. Zhang, J. Yu, M. Jaroniec, S.Z. Qiao, *Chem. Soc. Rev.* 43 (2014) 7787–7812.
- [12] W.C. Huang, L.M. Lyu, Y.C. Yang, M.H. Huang, *J. Am. Chem. Soc.* 134 (2012) 1261–1267.

[13] M. Barroso, A.J. Cowan, S.R. Pendlebury, M. Grätzel, D.R. Klug, J.R. Durrant, *J. Am. Chem. Soc.* 133 (2011) 14868–14871.

[14] F. Wang, C. Di Valentin, G. Pacchioni, *ChemCatChem* 4 (2012) 476–478.

[15] Y. Liu, Y. Deng, Z. Sun, J. Wei, G. Zheng, A.M. Asiri, S.B. Khan, M.M. Rahman, D. Zhao, *Small* 9 (2013) 2702–2708.

[16] W. Wu, G. Liu, Q. Xie, S. Liang, H. Zheng, R. Yuan, W. Su, L. Wu, *Green Chem.* 14 (2012) 1705–1709.

[17] Y. Hu, X. Gao, L. Yu, Y. Wang, J. Ning, S. Xu, X.W.D. Lou, *Angew. Chem.* 125 (2013) 5746–5749.

[18] J. Yu, Y. Yu, P. Zhou, W. Xiao, B. Cheng, *Appl. Catal. B: Environ.* 156 (2014) 184–191.

[19] Y. Zhou, Z. Tian, Z. Zhao, Q. Liu, J. Kou, X. Chen, J. Gao, S. Yan, Z. Zou, *ACS Appl. Mater. Interfaces* 3 (2011) 3594–3601.

[20] H. Li, J. Shang, Z. Ai, L. Zhang, *J. Am. Chem. Soc.* 137 (2015) 6393–6399.

[21] Y. Lei, G. Wang, S. Song, W. Fan, M. Pang, J. Tang, H. Zhang, *Dalton Trans.* 39 (2010) 3273–3278.

[22] X. Wang, K. Maeda, X. Chen, K. Takanabe, K. Domen, Y. Hou, X. Fu, M. Antonietti, *J. Am. Chem. Soc.* 131 (2009) 1680–1681.

[23] W. Zhang, Y. Wang, Z. Wang, Z. Zhong, R. Xu, *Chem. Commun.* 46 (2010) 7631–7633.

[24] G.-S. Li, D.-Q. Zhang, J.C. Yu, *Environ. Sci. Technol.* 43 (2009) 7079–7085.

[25] C.Y. Jimmy, L. Wu, J. Lin, P. Li, Q. Li, *Chem. Commun.* (2003) 1552–1553.

[26] J. Fu, B. Chang, Y. Tian, F. Xi, X. Dong, *J. Mater. Chem. A* 1 (2013) 3083–3090.

[27] A. Cao, Z. Liu, S. Chu, M. Wu, Z. Ye, Z. Cai, Y. Chang, S. Wang, Q. Gong, Y. Liu, *Adv. Mater.* 22 (2010) 103–106.

[28] Q. Li, B. Guo, J. Yu, J. Ran, B. Zhang, H. Yan, J.R. Gong, *J. Am. Chem. Soc.* 133 (2011) 10878–10884.

[29] T. Jia, A. Kolpin, C. Ma, R.C. Chan, W.M. Kwok, S.C. Tsang, *Chem. Commun.* 50 (2014) 1185–1188.

[30] J. Zhang, Y. Wang, J. Jin, J. Zhang, Z. Lin, F. Huang, J. Yu, *ACS Appl. Mater. Interfaces* 5 (2013) 10317–10324.

[31] Z. Chen, S. Liu, M.Q. Yang, Y.J. Xu, *ACS Appl. Mater. Interfaces* 5 (2013) 4309–4319.

[32] M. Li, X.-F. Yu, S. Liang, X.-N. Peng, Z.-J. Yang, Y.-L. Wang, Q.-Q. Wang, *Adv. Funct. Mater.* 21 (2011) 1788–1794.

[33] M.J. Nalbandian, K.E. Greenstein, D. Shuai, M. Zhang, Y.-H. Choa, G.F. Parkin, N.V. Myung, D.M. Cwiertny, *Environ. Sci. Technol.* 49 (2015) 1654–1663.

[34] X. Bai, R. Zong, C. Li, D. Liu, Y. Liu, Y. Zhu, *Appl. Catal. B: Environ.* 147 (2014) 82–91.

[35] F. Dong, T. Xiong, Y. Sun, Z. Zhao, Y. Zhou, X. Feng, Z. Wu, *Chem. Commun.* 50 (2014) 10386–10389.

[36] S. Weng, B. Chen, L. Xie, Z. Zheng, P. Liu, *J. Mater. Chem. A* 1 (2013) 3068.

[37] X. Liu, H. Cao, J. Yin, *Nano Res.* 4 (2011) 470–482.

[38] Z. Zhao, W. Zhang, Y. Sun, J. Yu, Y. Zhang, H. Yan, F. Dong, Z. Wu, *J. Phys. Chem. C* 120 (2016) 11889–11898.

[39] F. Dong, Z. Zhao, Y. Sun, Y. Zhang, S. Yan, Z. Wu, *Environ. Sci. Technol.* 49 (2015) 12432–12440.

[40] C. Wang, Y. Ao, P. Wang, J. Hou, J. Qian, S. Zhang, *Mater. Lett.* 64 (2010) 439–441.

[41] J. Cao, B. Xu, H. Lin, B. Luo, S. Chen, *Dalton Trans.* 41 (2012) 11482–11490.

[42] G. Yang, W. Yan, Q. Zhang, S. Shen, S. Ding, *Nanoscale* 5 (2013) 12432–12439.

[43] K. Cheng, W. Sun, H.-Y. Jiang, J. Liu, J. Lin, *J. Phys. Chem. C* 117 (2013) 14600–14607.

[44] Q. Zhang, Y. Zhou, F. Wang, F. Dong, W. Li, H. Li, G.R. Patzke, *J. Mater. Chem. A* 2 (2014) 11065–11072.

[45] H. Cheng, B. Huang, J. Lu, Z. Wang, B. Xu, X. Qin, X. Zhang, Y. Dai, *Phys. Chem. Chem. Phys.* 12 (2010) 15468–15475.

[46] F. Dong, Q. Li, Y. Sun, W.-K. Ho, *ACS Catal.* 4 (2014) 4341–4350.

[47] B. Cheng, Y. Le, J. Yu, J. Hazard. Mater. 177 (2010) 971–977.

[48] X. Gao, H.B. Wu, L. Zheng, Y. Zhong, Y. Hu, X.W.D. Lou, *Angew. Chem. Int. Ed.* 53 (2014) 5917–5921.

[49] Z. Zhao, W. Zhang, X. Lv, Y. Sun, F. Dong, Y. Zhang, *Environ. Sci.: Nano* 3 (2016) 1306–1317.

[50] W.H. Feng, Z.X. Pei, Z.B. Fang, M.L. Huang, M.L. Lu, S.X. Weng, Z.Y. Zheng, J. Hu, P. Liu, *J. Mater. Chem. A* 2 (2014) 7802.

[51] J. Li, S.K. Cushing, J. Bright, F. Meng, T.R. Senty, P. Zheng, A.D. Bristow, N. Wu, *ACS Catal.* 3 (2012) 47–51.

[52] L.-T. Guo, Y.-Y. Cai, J.-M. Ge, Y.-N. Zhang, L.-H. Gong, X.-H. Li, K.-X. Wang, Q.-Z. Ren, J. Su, J.-S. Chen, *ACS Catal.* 5 (2014) 388–392.

[53] Y. Yu, C. Cao, H. Liu, P. Li, F. Wei, Y. Jiang, W. Song, *J. Mater. Chem. A* 2 (2014) 1677–1681.

[54] J. Di, J. Xia, S. Yin, H. Xu, L. Xu, Y. Xu, M. He, H. Li, *J. Mater. Chem. A* 2 (2014) 5340.

[55] A. Leelavathi, G. Madras, N. Ravishankar, *J. Am. Chem. Soc.* 136 (2014) 14445–14445.

[56] W. Li, D. Li, W. Zhang, Y. Hu, Y. He, X. Fu, *J. Phys. Chem. C* 114 (2010) 2154–2159.

[57] J. Di, J. Xia, Y. Ge, L. Xu, H. Xu, M. He, Q. Zhang, H. Li, *J. Mater. Chem. A* 2 (2014) 15864–15874.

[58] H. Fang, Y. Gao, G. Li, J. An, P.-K. Wong, H. Fu, S. Yao, X. Nie, T. An, *Environ. Sci. Technol.* 47 (2013) 2704–2712.

[59] S.Y. Chai, Y.J. Kim, M.H. Jung, A.K. Chakraborty, D. Jung, W.I. Lee, *J. Catal.* 262 (2009) 144–149.

[60] N. Zhang, Y. Zhang, X. Pan, M.-Q. Yang, Y.-J. Xu, *J. Phys. Chem. C* 116 (2012) 18023–18031.

[61] Y. Xu, M.A. Schoonen, *Am. Mineral.* 85 (2000) 543–556.

[62] W. Wang, X. Chen, G. Liu, Z. Shen, D. Xia, P.K. Wong, J.C. Yu, *Appl. Catal. B: Environ.* 176–177 (2015) 444–453.

[63] Q. Xiang, J. Yu, B. Cheng, H. Ong, *Chem.—Asian J.* 5 (2010) 1466–1474.

[64] H. Bader, V. Sturzenegger, J. Hoigne, *Water Res.* 22 (1988) 1109–1115.

[65] Y. Gao, Y. Huang, Y. Li, Q. Zhang, J.-j. Cao, W. Ho, S.C. Lee, *ACS Sustain. Chem. Eng.* 4 (2016) 6912–6920.

[66] F. Dong, T. Xiong, S. Yan, H. Wang, Y. Sun, Y. Zhang, H. Huang, Z. Wu, *J. Catal.* 344 (2016) 401–410.

[67] T. Hirakawa, Y. Nosaka, *Langmuir: ACS J. Surf. Colloids* 18 (2002) 3247–3254.